Research Square

Preprints are preliminary reports that have not undergone peer review.
They should not be considered conclusive, used to inform clinical practice,
or referenced by the media as validated information.

Glioblastoma Cells with Adaptive Temozolomide Resistance andAbsent MGMT Expression Exhibit Enhanced Susceptibility to Zika Virus Oncolysis

Isabela Granha

isabelagranha@gmail.com

Universidade de São Paulo

Gustavo Sartorelli

Universidade de São Paulo

Letícia Maria de Oliveira Magalhães

Universidade de São Paulo

Desirée Plaça

Stanford University

Brandow Willy

Universidade de São Paulo

Alice Kei Endo

Universidade de São Paulo

Maria José Ferreira Alves

Universidade de São Paulo

Miyuki Uno

Universidade de São Paulo

Iuri Santana Neville

Universidade de São Paulo

Roger Chammas

Universidade de São Paulo

Elisa Helena Farias Jandrey

Universidade de São Paulo

Oswaldo Keith Okamoto

Universidade de São Paulo

Research Article

Keywords: Glioblastoma, Oncolytic virotherapy, Zika virus, Temozolomide resistance, MGMT, DNA damage response

Posted Date: November 13th, 2026

DOI: https://doi.org/10.21203/rs.3.rs-11445943/v1

License: This work is licensed under a Creative Commons Attribution 4.0 International License.
Read Full License

Additional Declarations: Competing interest reported. OKO is a co-founder of Vyrobiotherapeutics. All other authors have no relevant financial or non-financial interests to disclose.

Original article

Glioblastoma Cells with Adaptive Temozolomide Resistance and Absent *MGMT* Expression Exhibit Enhanced Susceptibility to Zika Virus Oncolysis

Isabela Granha[1*], Gustavo Sartorelli[1], Letícia Maria de Oliveira Magalhães[1], Desirée Plaça[2], Brandow Willy[1], Alice Kei Endo[1], Maria José Ferreira Alves[3,4], Miyuki Uno[3,4], Iuri Santana Neville[5,6], Roger Chammas[3,4], Elisa Helena Farias Jandrey[1*], Oswaldo Keith Okamoto[1*]

1. Centro de Estudos do Genoma Humano e Células-Tronco, Departamento de Genética e Biologia Evolutiva, Instituto de Biociências, Universidade de São Paulo, São Paulo, Brasil.

2. Department of Medicine, Division of Infectious Diseases and Geographic Medicine, and Department of Microbiology and Immunology, Stanford University, California, USA.

3. Center for Translational Research in Oncology (LIM24), Instituto do Câncer do Estado de São Paulo (ICESP), Hospital das Clínicas da Faculdade de Medicina da Universidade de São Paulo (HCFMUSP), São Paulo, São Paulo, Brasil.

4. Comprehensive Center for Precision Oncology, Universidade de São Paulo, São Paulo, São Paulo, Brasil.

5. Department of Neurosurgery, University of São Paulo, São Paulo, São Paulo, Brasil.

6. Instituto do Câncer do Estado de São Paulo – Hospital das Clínicas da Faculdade de Medicina da Universidade de São Paulo, São Paulo, São Paulo, Brasil.

*Corresponding authors:

isabelagranha@gmail.com, ORCID: https://orcid.org/0000-0002-3180-3039

elisajandrey@gmail.com, ORCID: https://orcid.org/0000-0003-0750-7552

keith.okamoto@usp.br, ORCID: https://orcid.org/0000-0002-8528-6225

Abstract

Purpose: Glioblastoma (GBM) resistance to temozolomide (TMZ) is a major barrier to durable disease control, and oncolytic virotherapy with Zika virus (ZIKV) has emerged as an alternative. However, given that host DNA damage response (DDR) appears to modulate virotherapy efficacy, whether ZIKV remains effective under TMZ resistance and its molecular determinants are open questions. We investigated the interplay between TMZ resistance and ZIKV infection in GBM, evaluating MGMT, the strongest clinical predictor of TMZ response and principal determinant of alkylation-damage repair, as a candidate shared determinant.

Methods: Six GBM cell lines were exposed to escalating TMZ doses to model acquired chemoresistance and characterized for ZIKV replication and induced cell death. Transcriptomic profiling, RT-qPCR, and pharmacological MGMT inhibition interrogated mechanistic links between DNA repair and viral susceptibility. Findings were validated in patient-derived organoids from two donors with discordant patterns of *MGMT* expression.

Results: Cells from four out of six GBM lines proliferated in vitro throughout TMZ exposure; U251 and U87 cells acquired resistance (adaptive, ADA), while U138 and LN18 cells showed unchanged IC50 (non-adaptive, N-ADA). Although acquisition of TMZ resistance did not alter susceptibility to ZIKV oncolysis, remarkably, ADA lines were more susceptible to ZIKV-induced death and supported higher viral replication than N-ADA lines. ADA cells lacked *MGMT* expression and showed basal depletion of DNA repair programmes, while N-ADA cells expressed both. Pharmacological MGMT inhibition sensitized N-ADA LN18 cells to ZIKV with concurrent γH2AX accumulation, supporting a contributing role for MGMT-dependent repair. This dichotomy was recapitulated in ZIKV infection assays with patient-derived GBM organoids displaying opposite patterns of *MGMT* expression.

Conclusion: *MGMT* status may be a common indicator of TMZ or ZIKV response in GBM, supporting its use for future rational combination ZIKV virotherapy tailored to patient *MGMT* expression.

Keywords

Glioblastoma, Oncolytic virotherapy, Zika virus, Temozolomide resistance, MGMT,

DNA damage response

Acknowledgements

We thank Prof. Mayana Zatz for funding the RNA sequencing experiments, and Raiane Ferreira and Mah Hui Ling for technical support with RNA-seq processing. We thank Prof. Carlos Federico Menck for providing the U251 MG cell line, MGMT inhibitor and the anti-γH2AX antibody used in this study. We also thank Bio-Manguinhos/Fiocruz for kindly donating the anti-ZIKV antibody. We also thank Prof. Prof. Luís Carlos de Souza Ferreira for donating a vial of ZIKV-17 that has been expanded for use in this project.

This work was supported by the São Paulo Research Foundation (FAPESP) through the Center for Research on the Human Genome and Stem Cells (CEPID, grant 2013/14178-8, Institute of Biosciences, University of São Paulo) and by the Coordenação de Aperfeiçoamento de Pessoal de Nível Superior – Brasil (CAPES). I.G. was supported by a master's fellowship from FAPESP (grant 2023/02209-6) and CAPES (PROEX process 88887.822363/2023-0). L.M.O.M. was supported by FAPESP (grant 24/19387-7). E.H.F.J. was supported by FAPESP (grant 2021/04323-5).

1. Introduction

Glioblastoma (GBM) is a highly aggressive and heterogeneous brain tumor, and despite sustained research efforts, few treatment alternatives have been approved over the last two decades [1]. The current standard of care, established by Stupp in 2005 [2], consists of maximal safe tumor resection followed by radiotherapy with concomitant and adjuvant chemotherapy with temozolomide (TMZ). This regimen extends median overall survival from approximately 12 to 15 months [2], and second-line alternatives offer only marginal additional benefit [1]. Tumor recurrence is virtually inevitable [3], and the emergence of a TMZ-resistant phenotype represents a major barrier to durable disease control.

A key contributor to TMZ resistance is O^6-methylguanine-DNA methyltransferase (MGMT), a DNA repair enzyme that directly reverses drug-induced DNA lesions [4]. MGMT underlies two distinct resistance phenotypes in patient-derived IDH-wt GBM

cells: an "adaptive" (ADA) response, which retains partial responsiveness to TMZ, and a "non-adaptive" (N-ADA) response, refractory even at higher doses, with substantially greater *MGMT* expression than ADA [5]. Clinically, 82% of chemotherapy-resistant GBM samples harbor unmethylated *MGMT* promoters, whereas 89% of responsive tumors are methylated [6], and patients with methylated *MGMT* promoters achieve significantly longer survival following radiochemotherapy [7]. *MGMT* status therefore functions as both a mechanistic driver of TMZ resistance and the strongest clinical predictor of GBM response to standard care.

Given the limited efficacy of conventional treatment, oncolytic virotherapy has gained increasing translational interest. Preclinical studies have demonstrated activity of several oncolytic viruses against TMZ-resistant GBM cells [8,9], and the recent clinical approval of the modified herpes simplex virus G47Δ for recurrent GBM in Japan [10] validated this platform as a viable therapeutic modality. Beyond herpes-based approaches, Zika virus (ZIKV) has emerged as a promising candidate for GBM and other central nervous system tumors due to its selective tropism for neural precursor and glioma stem cells [11–14], and prior work has demonstrated additive effect with TMZ in glioma stem cell models [11].

Notably, host DNA damage response (DDR) capacity is emerging as a key modulator of oncolytic virus efficacy: viral infection frequently induces DNA damage in host cells [15], and ZIKV specifically triggers DDR activation via direct interference of viral proteins or oxidative stress and deoxynucleoside triphosphate depletion [16,17]. Pharmacological suppression of DDR pathways potentiates oncolytic activity across multiple viral platforms in GBM, including HSV G47Δ combined with MGMT inhibitors [18] and VSVΔ51 or ZIKV combined with CDK4/6 inhibitors [19]. Because MGMT is the principal determinant of alkylation-damage repair in GBM and the strongest clinical predictor of the TMZ response, we hypothesised that *MGMT* expression may also influence ZIKV oncolysis, offering a molecularly rational biomarker for combination therapy design.

Here, we modeled acquired TMZ resistance in a panel of GBM cell lines, explored intrinsic TMZ response heterogeneity through the ADA/N-ADA framework, and identified MGMT as a shared molecular determinant of both TMZ and ZIKV

susceptibility. Findings were validated in patient-derived GBM organoids with discordant *MGMT* expression pattern, and a contributing role for MGMT-dependent DNA repair was established using pharmacological inhibition, positioning *MGMT* expression as a clinically actionable biomarker for ZIKV virotherapy.

2. Materials and Methods

2.1. Cell Culture

Six commercial GBM cell lines were used: U87 MG, A172, U343, and LN18 (ATCC); U251 MG (donated by Prof. Carlos Menck, USP); and U138 MG (donated by Vyro Biotherapeutics). VERO cells (Cell Bank of Rio de Janeiro) were used for viral titration. Cells were maintained in DMEM with GlutaMAX, 10% FBS, 1× antibiotic-antimycotic (all Gibco), and 1× Normocin (InvivoGen); 3D tumor spheres were generated in 96-well low-adhesion plates. Cultures were tested periodically for mycoplasma (MycoAlert Plus, Lonza). Detailed protocols are in Supplementary Methods.

2.2. TMZ-resistance induction and senescence

GBM cell lines were exposed to escalating doses of TMZ (T2577, Sigma-Aldrich; 5, 10, 20, 40 μM) over 28 days, mimicking clinical levels [2,20]. Control cells received equivalent DMSO. Resistant (R) and control (CTRL) cells were expanded in the TMZ-free medium; all experiments used cells within five passages post-treatment. Senescence was assessed at passage 1 with the Senescence-Associated β-Galactosidase Staining Kit (cat. no. 9860, Cell Signaling Technology).

2.3. ZIKV production and infection

Viral stocks of ZIKV-17 (GenBank: MH882527.1) were produced from passage 5 [21,22]. Stock titer, determined by plaque-forming unit (PFU) assay, was 4.44×10^5 PFU/mL (n = 6). For infection, cells were seeded in appropriate plate formats and inoculated 24 h later with ZIKV at the indicated MOI in DMEM without supplements. After 1 h of adsorption at 37 °C, the inoculum was replaced with complete medium. Detailed seeding densities and volumes per format are in Supplementary Methods.

2.4. Cell viability and death assays

TMZ resistance was assessed by MTT dose–response curves (1 to 1024 µM, 6 days). ZIKV cytotoxicity was evaluated at MOIs of 0.01–2 at 72 hpi using MTT (Sigma-Aldrich), read at 570 nm (Epoch, Agilent). Population growth was monitored on the xCELLigence RTCA system (Agilent). Cell death was assessed at 24, 48, and 72 hpi using the LIVE/DEAD Kit (cat. no. L3224, Thermo) for both monolayer and 3D cultures, imaged on a BioTek Cytation C10 (Agilent) and quantified with custom Python scripts. For apoptosis and necrosis, cells and supernatants at 72 hpi were stained with the Dead Cell Apoptosis Kit (Annexin V AF488 and PI; cat. no. V13242, Thermo) and acquired on a FACSymphony A1 (BD; 50,000 events per sample); gates in FlowJo were set relative to MOCK.

2.5. Quantification of viral replication

Supernatants collected at 48 hpi were processed for infectious titer (PFU assay[23]) and viral RNA quantification. RNA was extracted with the QIAamp Viral RNA Mini Kit (Qiagen) and amplified with the TaqMan One-Step RT-PCR system (Thermo) on a 7500 Fast Real-Time PCR System (Applied Biosystems), targeting the ZIKV envelope gene. Absolute copy numbers were derived from a standard curve (10^1 to 10^8 copies/µL) generated from a synthetic gBlock (IDT). Primer/probe sequences and cycling conditions are in Supplementary Table 1.

2.6. Gene expression by RT-qPCR

Total RNA was extracted from CTRL and R cells at ~70% confluence, 48 h post-ZIKV infection, using the RNeasy Mini Kit (Qiagen). Reverse transcription used SuperScript III (Life Technologies), and RT-qPCR was performed on a 7500 Real-Time PCR System with SYBR Green Master Mix (Thermo). Expression was normalized to GAPDH using the 2^−ΔΔCt method. Primers are listed in Supplementary Table 1.

2.7. Immunocytochemistry

At 48 hpi, cells were fixed in 3.7% formaldehyde and processed for immunofluorescence with primary antibodies against ZIKV (1:250, anti-flavivirus, Biomanguinhos), GFAP (1:400, Sigma-Aldrich, G9269), and γH2AX (1:400, Abcam).

Secondary antibodies were AF488 anti-mouse and AF647 anti-rabbit (1:500, Thermo), with DAPI counterstain. Images were acquired on a BioTek Cytation C10 (Agilent) and quantified with custom Python scripts. Full staining protocol is in Supplementary Methods.

2.8. MGMT inhibition

O^6-benzylguanine (O^6-BG; Merck) was dissolved in DMSO. LN18 and U138 cells were pre-treated with 25 or 50 µM O^6-BG, or DMSO, for 1 h prior to ZIKV infection (MOI 0.5). O^6-BG was maintained in the post-infection medium. Viability was assessed by MTT at 72 hpi and viral particles by RT-qPCR.

2.9. Patient-derived glioblastoma organoid (GBOs)

GBOs were generated from two GBM specimens (Patients 11939 and 11947) obtained under institutional ethics approval (CAAE: 20271719.8.0000.0065), following Jacob et al. (2020)[24]. When organoids reached ~0.5 mm in cross-sectional area, individual GBOs were plated one per well in 96-well plates and infected with 10,000 PFU of ZIKV per organoid for 72 h. Individual GBOs served as experimental replicates for viability, viral titration, and immunofluorescence. Viability was measured with CellTiter-Glo (Promega, G7570) on a Lucetta Luminometer (Lonza) and normalized to organoid area. Whole-mount immunofluorescence used anti-ZIKV (1:200, Biomanguinhos) and anti-GFAP (1:400, Sigma-Aldrich), imaged on a Zeiss LSM 800 confocal microscope. Detailed protocols are in Supplementary Methods.

2.10. Histopathology

H&E and IHC of patient tumor samples were performed by the Department of Pathology at ICESP as part of the institutional diagnostic workflow, assessing GFAP, p53, and Ki-67.

2.11. RNA-sequencing

Total RNA from U251, U87, LN18, and U138 was extracted with the RNeasy Mini Kit (Qiagen); integrity was verified on a Bioanalyzer (RIN > 8.0). In-house data were integrated with CCLE datasets for U87 MG and U251 MG. Batch effects were

corrected using ComBat (*sva* R package, R v4.3.2). Differential expression (CTRL vs R) was performed on the ExpressAnalyst platform ($log_2FC > 0.5$, adjusted $p < 0.05$). GSEA against Reactome and visualization as ridgeline plots were performed within ExpressAnalyst. MGMT and DNA-repair gene sets were expanded via Enrichr (ARCHS4 co-expression matrix; GeneRIF gene-gene co-mention matrix)[25]. Heatmaps were generated in Morpheus with Euclidean distance and complete-linkage clustering. Cumulative distributions were computed with the *ecdf* function (*stats* R package).

2.12. Statistical analysis

Normality was tested using Shapiro–Wilk. Parametric data are presented as mean ± SD and analyzed by Student's t-test (with Welch's correction where appropriate), one-way ANOVA with Dunnett's multiple comparisons, two-way ANOVA, or multiple t-tests with Holm–Šídák or Dunnett post-hoc correction. Non-parametric data are presented as boxplots and analyzed by Mann–Whitney test. Data represent a minimum of three independent biological replicates, unless specified. Significance was defined as $p < 0.05$. Analyses were performed in GraphPad Prism v9.0.

3. Results

3.1. Induced TMZ-resistance does not change GBM cells' susceptibility to ZIKV infection and oncolysis

To model acquired chemoresistance, we exposed six GBM cell lines to escalating, clinically relevant doses of TMZ (5-40 µM) over 28 days. A172 and U343 cells failed to complete the regimen due to early senescence and growth arrest (Figure S1A,B), whereas U251, U87, U138, and LN18 cells proliferated throughout, exhibiting minimal β-galactosidase marking (Figure S1C,D). These lines, hereafter termed CTRL (DMSO-treated) or R (TMZ-treated), were then assessed for TMZ sensitivity. Dose-response assays revealed a significant increase in IC50 for R cells compared to CTRL in U251 and U87 (6.7 and 2.5-fold, respectively), but not in U138 and LN18 (Figure 1A). Transcriptomic analysis of U251 and U87 R *versus* CTRL revealed an enrichment in pathways related to cell proliferation and cell cycle (Figure 1B).

We next asked how TMZ-resistant cells respond to ZIKV. Infection of monolayer cells resulted in identical rates of apoptosis and necrosis between CTRL and R counterparts across all lines (Figure 1C), and viral titers and total RNA levels were also comparable (Figure 1D-E). In a more physiologically relevant context, although U87-CTRL tumor spheres were larger and fewer than U87-R (Figure S2A-C), ZIKV infection induced equivalent cell death in both CTRL and R spheres across all four cell lines (Figure 1F, Figure S2D-F).

3.2. Adaptative and non-adaptative resistance responses to TMZ mirror ZIKV-infection susceptibility

Despite the absence of correlation between induced TMZ resistance and ZIKV infection, the cell lines presented disparate baseline responses to TMZ. This heterogeneity has been described in patient-derived GBM cells maintained under sub-lethal TMZ, where half develop adaptive resistance (associated with glioma stem cell expansion) while the remainder display an intrinsic, non-adaptive phenotype (enriched in cell cycle regulation and DNA repair pathways)[5].

Under this criterion, U251 and U87 cells were assigned as adaptive (ADA) responders (increased IC50), while U138 and LN18 cells exhibited an intrinsic non-adaptive (N-ADA) response (unchanged IC50) (Figure 2A). Strikingly, this classification unveiled a major determinant of ZIKV efficacy: ADA lines exhibited significantly greater loss of viability and impaired growth post-ZIKV infection than N-ADA lines (Figure 2B,C), lower proportions of viable cells and higher necrosis upon ZIKV infection (Figure 2D,E), and supported higher levels of viral replication - with more viable viral particles, higher viral RNA, and a greater percentage of infected cells (Figure 2F-G). This differential response was partially maintained in 3D culture: ADA cells displayed overall increased cell death compared to N-ADA cells (Figure 2H), while ZIKV replication showed no differences (Figure 2I).

We hypothesized that the molecular distinction between ADA and N-ADA groups could underlie the differential ZIKV susceptibility. Indeed, RT-qPCR analysis revealed that ADA cells lacked *MGMT* expression, whereas N-ADA cells expressed it robustly (Figure 3A). Transcriptomic analysis of all four cell lines confirmed that gene sets for *MGMT* co-expression and DNA repair were basally enriched in N-ADA compared to

ADA cells (Figure 3B,C), with consistently higher expression of individual genes within these pathways (Figure 3D).

3.3. DNA damage response influences response to ZIKV in glioblastoma organoids

To validate our findings in a patient-relevant context, we established GBOs from two primary tumors (Patients 11947 and 11939; Supplementary Table 2). Tumor tissue sections were positive for GFAP and exhibited a high proliferative index (Ki-67 > 50%) (Figure S3). Consistent with our cell line classification, GBOs from Patient 11939 were *MGMT*-negative (ADA-like), while those from Patient 11947 were *MGMT*-positive (N-ADA-like) (Figure 4A).

Upon ZIKV infection, *MGMT*-negative 11939 GBOs exhibited significantly decreased viability compared to *MGMT*-positive 11947 GBOs (Figure 4B), although extracellular viral titers were comparable between organoid lines (Figure 4C). Nevertheless, 11939 ADA-like GBOs displayed a larger ZIKV-positive area than 11947 N-ADA-like GBOs (34.94% versus 11.77%, respectively; Figure 4D). These findings reproduce the ADA/N-ADA dichotomy observed in GBM lines and suggest that, in 3D tumor models, ZIKV-induced cytotoxicity may not directly correlate with extracellular viral output.

To establish a causal role for MGMT, we pharmacologically inhibited it in the N-ADA line LN18. While neither the MGMT inhibitor (iMGMT, 50 µM) nor ZIKV (MOI 0.5) alone affected viability, their combination reduced cell viability (Figure 5A) - a feature not observed with a lower iMGMT dose (25 µM) and ZIKV MOI 0.5 (Figure S4A). This impaired viability was accompanied by increased ZIKV production (Figure 5B) and a marked increase in DNA damage measured by γH2AX foci (Figure 5C-D). In contrast, MGMT inhibition failed to enhance ZIKV-induced cytotoxicity or viral production in U138 cells (Figure S4B).

4. Discussion

In the present study, we identify *MGMT* expression as a shared molecular determinant of TMZ and ZIKV response in GBM. Across established GBM cell lines and patient-derived organoids, low-*MGMT* tumors were susceptible, while *MGMT*-expressing tumors were resistant to both modalities. Pharmacological MGMT inhibition converted a resistant GBM line into a ZIKV-susceptible phenotype with concurrent accumulation

of DNA damage, establishing a link between *MGMT*-dependent DNA repair and viral oncolysis. These findings position ZIKV virotherapy as a complementary modality that can be rationally combined with standard of care or tailored to patient-specific *MGMT* expression.

Our data reproduce and extend the ADA/N-ADA[5]. Rather than merely dictating chemotherapy outcomes, intrinsic resistance to TMZ appears to cross-protect against ZIKV oncolysis, with ADA cells supporting substantially higher levels of viral replication and undergoing greater ZIKV-induced cell death than N-ADA cells. This convergence across independent datasets suggests that ADA/N-ADA reflects a fundamental cell-state distinction with therapeutic consequences beyond TMZ alone. Because our observations derive from four established cell lines, prospectively applying the ADA/N-ADA framework to a larger patient-derived cohort stratified by *MGMT* status and profiled for ZIKV response would provide a rigorous test of this dichotomy as a predictive tool for oncolytic virotherapy selection.

Mechanistically, our results point to *MGMT*-dependent DNA repair capacity as a driver of this divergence. Viral entry and replication routinely trigger host DDR pathways that either restrict infection or, when overwhelmed, precipitate cell death [26]. Although ZIKV is an RNA virus, its infection has been associated with DNA damage and S-phase cell cycle arrest in neural progenitor cells[16], and with double-strand break induction in GBM cell lines through the action of the viral NS2B/NS3 protease [17]. Consistent with this framework, ADA cells lacked *MGMT* expression and exhibited basal depletion of DNA repair transcriptional programs, rendering them vulnerable to ZIKV-induced DNA damage, whereas N-ADA cells robustly expressed *MGMT* and its co-regulated repair machinery, buffering the viral-induced stress.

Pharmacological MGMT inhibition in the N-ADA line LN18 sensitized these cells to ZIKV, with combined treatment yielding synergistic viability loss, increased viral output, and elevated γH2AX foci compared with the vehicle control. This rescue supports MGMT-dependent alkylation repair as a targetable axis for ZIKV virotherapy and aligns with an emerging body of work showing that DDR suppression potentiates oncolytic viruses in GBM. As example, CDK4/6 inhibition with abemaciclib synergizes with the oncolytic VSVΔ51 in monotherapy-resistant GBM lines and with ZIKV against glioma

stem cells[19], and MGMT inhibition sensitizes TMZ-refractory glioma stem cells to combined oncolytic HSV G47Δ and TMZ through amplified double-strand break formation and DDR sequestration[18].

A notable exception was U138, which was not sensitised by MGMT inhibition despite its N-ADA classification. This likely reflects U138's higher baseline expression of MGMT and DNA repair components compared with LN18 (Figure 3D), which may raise the pharmacological threshold required to impair alkylation-damage repair; higher iMGMT doses may therefore be needed for comparable sensitization. Additional cell-intrinsic factors may also modulate ZIKV response. Although human GBM cell lines including U138 express key ZIKV entry receptors such as AXL and integrin αvβ5 [27], downstream replication depends on host defense mechanisms, and baseline type I interferon (IFN-I) activation inversely correlates with ZIKV susceptibility in GBM [28,29]. Importantly, DDR and innate immune signaling are interconnected, with DNA damage sensors such as ATM and cytosolic DNA fragments activating IFN-I production[30]. U138 might therefore sustain a more robust basal IFN-I tone that restricts ZIKV replication and blunts the effect of MGMT inhibitor co-treatment, warranting further mechanistic investigation.

Translating these findings into patient-derived organoids supported the *MGMT*-dependent dichotomy within a complex 3D tumor context. *MGMT*-negative organoids displayed significantly larger ZIKV-positive areas and reduced viability compared with *MGMT*-positive organoids, recapitulating the ADA/N-ADA divergence observed in cell lines. This concordance underscores patient-derived organoids as a reliable bridging model between conventional 2D cultures and clinical settings, retaining patient-specific cellular and molecular landscapes[24,31] and offering superior accuracy in evaluating drug response, notably outperforming *MGMT* promoter methylation status in predicting TMZ sensitivity [32]. Nevertheless, the small cohort (n = 2) precludes generalization, and larger organoid series will be required to formally validate *MGMT* expression as a predictive biomarker for ZIKV response.

Current GBM management relies heavily on *MGMT* status[7]. In tumors with methylated *MGMT* promoters, approximately 42% of newly diagnosed cases and those deriving the greatest benefit from TMZ[33], ZIKV oncolytic virotherapy may offer

additional benefit when combined with standard chemoradiotherapy, supported by evidence of additive effect between attenuated ZIKV and TMZ against glioma stem cells in vitro[11]. Moreover, our data support ZIKV oncolytic virotherapy for patients experiencing recurrent GBM after TMZ treatment cycle, given that acquisition of TMZ resistance did not alter sensitivity to ZIKV oncolysis in ADA cells. Patients with unmethylated MGMT tumors and predicted increased resistance to TMZ may also benefit from ZIKV oncolytic virotherapy, although higher viral doses may be required. Utilizing *MGMT* expression as a stratifying biomarker for ZIKV deployment thus represents a pragmatic translational strategy, hijacking a marker already integrated into standard GBM workflows [2].

Limitations of this study should be acknowledged. The patient-derived organoid cohort was restricted to two donors, and cell line work relied on immortalized lines that may not fully recapitulate primary tumor biology. In vivo validation of the proposed combination strategies remains outstanding, and formal rescue experiments, such as *MGMT* re-expression in ADA cells, would further strengthen causal inference beyond the γH2AX evidence presented here. In summary, *MGMT* expression emerges as a shared biomarker for TMZ and ZIKV response in GBM, offering a molecularly rational path toward combination oncolytic virotherapy tailored to patient *MGMT* status.

5. References

1. Fisher JP, Adamson DC. Current FDA-approved therapies for high-grade malignant gliomas. Biomedicines [Internet]. MDPI AG; 2021;9:324. https://doi.org/10.3390/biomedicines9030324

2. Stupp R, Mason WP, van den Bent MJ, Weller M, Fisher B, Taphoorn MJB, et al. Radiotherapy plus concomitant and adjuvant temozolomide for glioblastoma. N Engl J Med [Internet]. New England Journal of Medicine (NEJM/MMS); 2005;352:987–96. https://doi.org/10.1056/NEJMoa043330

3. Chang C, Chavarro VS, Gerstl JVE, Blitz SE, Spanehl L, Dubinski D, et al. Recurrent glioblastoma-molecular underpinnings and evolving treatment paradigms. Int J Mol Sci [Internet]. MDPI AG; 2024;25:6733. https://doi.org/10.3390/ijms25126733

4. Singh N, Miner A, Hennis L, Mittal S. Mechanisms of temozolomide resistance in glioblastoma - a comprehensive review. Canc Drug Resist [Internet]. OAE Publishing Inc.; 2021;4:17–43. https://doi.org/10.20517/cdr.2020.79

5. Fabro F, Kers TV, Feller KJ, Beerens C, Ntafoulis I, Idbaih A, et al. Genomic exploration of distinct molecular phenotypes steering temozolomide resistance development in patient-derived glioblastoma cells. Int J Mol Sci [Internet]. MDPI AG; 2023;24:15678. https://doi.org/10.3390/ijms242115678

6. Ntafoulis I, Kleijn A, Ju J, Jimenez-Cowell K, Fabro F, Klein M, et al. Ex vivo drug sensitivity screening predicts response to temozolomide in glioblastoma patients and identifies candidate biomarkers. Br J Cancer [Internet]. 2023;129:1327–38. https://doi.org/10.1038/s41416-023-02402-y

7. Wen PY, Weller M, Lee EQ, Touat M, Khasraw M, Rahman R, et al. Glioblastoma in adults: A Society for Neuro-Oncology (SNO) and European Society of Neuro-Oncology (EANO) consensus review on current management and future directions. Neuro Oncol [Internet]. Oxford University Press (OUP); 2025;27:2751–88. https://doi.org/10.1093/neuonc/noaf177

8. Jahan N, Lee JM, Shah K, Wakimoto H. Therapeutic targeting of chemoresistant and recurrent glioblastoma stem cells with a proapoptotic variant of oncolytic herpes simplex virus: Therapeutic targeting of chemoresistant GBM. Int J Cancer [Internet]. Wiley; 2017;141:1671–81. https://doi.org/10.1002/ijc.30811

9. Jiang B, Lun X, Hao X, Wang Y, Yin X, Huang D, et al. Temozolomide resistant human brain tumor stem cells are susceptible to recombinant vesicular stomatitis virus and double-deleted Vaccinia virus in vitro. Biomed Pharmacother [Internet]. Elsevier BV; 2017 [cited 2026 Sept 24];95:1201–8. https://doi.org/10.1016/j.biopha.2017.09.030

10. Todo T, Ito H, Ino Y, Ohtsu H, Ota Y, Shibahara J, et al. Intratumoral oncolytic herpes virus G47Δ for residual or recurrent glioblastoma: a phase 2 trial. Nat Med [Internet]. Springer Science and Business Media LLC; 2022;28:1630–9. https://doi.org/10.1038/s41591-022-01897-x

11. Zhu Z, Gorman MJ, McKenzie LD, Chai JN, Hubert CG, Prager BC, et al. Zika virus has oncolytic activity against glioblastoma stem cells. J Exp Med [Internet]. Rockefeller University Press; 2017;214:2843–57. https://doi.org/10.1084/jem.20171093

12. Kaid C, Goulart E, Caires-Júnior LC, Araujo BHS, Soares-Schanoski A, Bueno HMS, et al. Zika virus selectively kills aggressive human embryonal CNS tumor cells in vitro and in vivo. Cancer Res [Internet]. American Association for Cancer Research (AACR); 2018;78:3363–74. https://doi.org/10.1158/0008-5472.CAN-17-3201

13. Ferreira RO, Granha I, Ferreira RS, Bueno H de S, Okamoto OK, Kaid C, et al. Effect of serial systemic and intratumoral injections of oncolytic ZIKVBR in mice bearing embryonal CNS tumors. Viruses [Internet]. MDPI AG; 2021;13:2103. https://doi.org/10.3390/v13102103

14. Granha I, Sartorelli G, Okamoto OK, Jandrey EHF. Emergent and underexplored oncolytic viruses for treating pediatric central nervous system tumors. EJC Paediatr Oncol [Internet]. Elsevier BV; 2024;3:100151. https://doi.org/10.1016/j.ejcped.2024.100151

15. Song M, Wang S, Fei X, Guo G. Viral manipulation of DNA damage response signaling: molecular mechanisms and therapeutic implications. Virol Sin [Internet]. Elsevier BV; 2026; https://doi.org/10.1016/j.virs.2026.08.014

16. Hammack C, Ogden SC, Madden JC Jr, Medina A, Xu C, Phillips E, et al. Zika virus infection induces DNA damage response in human neural progenitors that enhances viral replication. J Virol [Internet]. American Society for Microbiology; 2019;93:e00638–19. https://doi.org/10.1128/JVI.00638-19

17. Wang Y, Song D, Li Y, Qin L, Wan Q, Hu H, et al. Erp57 facilitates ZIKV-induced DNA damage via NS2B/NS3 complex formation. Emerg Microbes Infect [Internet]. Informa UK Limited; 2024;13:2417864. https://doi.org/10.1080/22221751.2024.2417864

18. Kanai R, Rabkin SD, Yip S, Sgubin D, Zaupa CM, Hirose Y, et al. Oncolytic virus-mediated manipulation of DNA damage responses: synergy with chemotherapy in killing glioblastoma stem cells. J Natl Cancer Inst [Internet]. Oxford University Press (OUP); 2012;104:42–55. https://doi.org/10.1093/jnci/djr509

19. Xiao J, Liang J, Fan J, Hou P, Li X, Zhang H, et al. CDK4/6 inhibition enhances oncolytic virus efficacy by potentiating tumor-selective cell killing and T-cell activation in refractory glioblastoma. Cancer Res [Internet]. American Association for Cancer Research (AACR); 2022;82:3359–74. https://doi.org/10.1158/0008-5472.CAN-21-3656

20. Ostermann S, Csajka C, Buclin T, Leyvraz S, Lejeune F, Decosterd LA, et al. Plasma and cerebrospinal fluid population pharmacokinetics of temozolomide in malignant glioma patients. Clin Cancer Res [Internet]. American Association for Cancer Research (AACR); 2004;10:3728–36. https://doi.org/10.1158/1078-0432.CCR-03-0807

21. Cugola FR, Fernandes IR, Russo FB, Freitas BC, Dias JLM, Guimarães KP, et al. The Brazilian Zika virus strain causes birth defects in experimental models. Nature [Internet]. Springer Science and Business Media LLC; 2016;534:267–71. https://doi.org/10.1038/nature18296

22. Sumita LM, Rodrigues JP, Ferreira NE, Felix AC, Souza NCS, Machado CM, et al. DETECTION OF HUMAN ANTI-ZIKA VIRUS IgG BY ELISA USING AN ANTIGEN FROM in vitro INFECTED VERO CELLS: PRELIMINARY RESULTS. Rev Inst Med Trop Sao Paulo [Internet]. FapUNIFESP (SciELO); 2016;58:89. https://doi.org/10.1590/S1678-9946201658089

23. Baer A, Kehn-Hall K. Viral concentration determination through plaque assays: using traditional and novel overlay systems. J Vis Exp [Internet]. MyJove Corporation; 2014;e52065. https://doi.org/10.3791/52065

24. Jacob F, Salinas RD, Zhang DY, Nguyen PTT, Schnoll JG, Wong SZH, et al. A patient-derived glioblastoma organoid model and biobank recapitulates inter- and intra-tumoral heterogeneity. Cell [Internet]. Elsevier BV; 2020;180:188–204.e22. https://doi.org/10.1016/j.cell.2019.11.036

25. Kuleshov MV, Jones MR, Rouillard AD, Fernandez NF, Duan Q, Wang Z, et al. Enrichr: a comprehensive gene set enrichment analysis web server 2016 update. Nucleic Acids Res [Internet]. Oxford University Press (OUP); 2016;44:W90–7. https://doi.org/10.1093/nar/gkw377

26. Weitzman MD, Fradet-Turcotte A. Virus DNA replication and the host DNA damage response. Annu Rev Virol [Internet]. Annual Reviews; 2018;5:141–64. https://doi.org/10.1146/annurev-virology-092917-043534

27. Pöhlking C, Beier S, Formanski JP, Friese M, Schreiber M, Schwalbe B. Isolation of cells from glioblastoma multiforme grade 4 tumors for infection with Zika virus prME and ME pseudotyped HIV-1. Int J Mol Sci [Internet]. MDPI AG; 2023;24:4467. https://doi.org/10.3390/ijms24054467

28. Zhu Z, Mesci P, Bernatchez JA, Gimple RC, Wang X, Schafer ST, et al. Zika virus targets glioblastoma stem cells through a SOX2-integrin αvβ5 axis. Cell Stem Cell [Internet]. Elsevier BV; 2020;26:187–204.e10. https://doi.org/10.1016/j.stem.2019.11.016

29. Bulstrode H, Girdler GC, Gracia T, Aivazidis A, Moutsopoulos I, Young AMH, et al. Myeloid cell interferon secretion restricts Zika flavivirus infection of developing and malignant

human neural progenitor cells. Neuron [Internet]. Elsevier BV; 2022;110:3936–51.e10. https://doi.org/10.1016/j.neuron.2022.09.002

30. Tong J, Song J, Zhang W, Zhai J, Guan Q, Wang H, et al. When DNA-damage responses meet innate and adaptive immunity. Cell Mol Life Sci [Internet]. 2024;81:185. https://doi.org/10.1007/s00018-024-05214-2

31. Majc B, Habič A, Malavolta M, Vittori M, Porčnik A, Bošnjak R, et al. Patient-derived tumor organoids mimic treatment-induced DNA damage response in glioblastoma. iScience [Internet]. Elsevier BV; 2024;27:110604. https://doi.org/10.1016/j.isci.2024.110604

32. Park J, Qiu M, Cho EJ, Seo S, Moon J-H, Kim M, et al. Patient-derived organoids predict personalized drug response and reveal alternative therapeutic options in glioblastoma. Cell Rep Med [Internet]. Elsevier BV; 2026 [cited 2026 Sept 24];7:102850. https://doi.org/10.1016/j.xcrm.2026.102850

33. Barnett AE, Ozair A, Bamashmos AS, Li H, Bosler DS, Yeaney G, et al. MGMT methylation and differential survival impact by sex in glioblastoma. Cancers (Basel) [Internet]. MDPI AG; 2024;16:1374. https://doi.org/10.3390/cancers16071374

6. Statements & Declarations

Funding

This work was supported by the São Paulo Research Foundation (FAPESP) through the Center for Research on the Human Genome and Stem Cells (grant 2013/14178-8) and by the Coordenação de Aperfeiçoamento de Pessoal de Nível Superior – Brasil (CAPES). I.G. was supported by FAPESP (grant 2023/02209-6) and CAPES (PROEX 88887.822363/2023-0). E.H.F.J. was supported by FAPESP (grant 2021/04323-5).

Competing Interests

OKO is a co-founder of Vyrobiotherapeutics. All other authors have no relevant financial or non-financial interests to disclose.

Author Contributions

Conceptualization: I.G., E.H.F.J., O.K.O.; Methodology: I.G., E.H.F.J., G.S., L.M.O.M., D.P., B.W., A.K.E.; Investigation: I.G., G.S., L.M.O.M., D.P., B.W., A.K.E.; Resources: M.J.F.A., M.U., I.S.N., R.C., O.K.O.; Formal analysis: I.G., G.S., D.P.; Writing - original draft: I.G.; Writing - review and editing: I.G., G.S., E.H.F.J., O.K.O.; Supervision: E.H.F.J., O.K.O.; Funding acquisition: O.K.O.

Data Availability

The datasets generated and/or analysed during the current study are available from the corresponding author on reasonable request.

Ethics approval

This study was performed in line with the principles of the Declaration of Helsinki. The study protocol was approved by the Ethics Committee of Instituto do Câncer do Estado de São Paulo (ICESP), CAAE: 20271719.8.0000.0065. All patients provided written informed consent for donation of tumor tissue used in this study.

Consent to participate

Informed consent was obtained from all individual participants included in the study.

Consent to publish

Not applicable. The manuscript does not contain any individually identifiable data or images of study participants.

7. Figures Captions

Figure 1. Acquisition of temozolomide resistance does not alter susceptibility of GBM cells to ZIKV infection

(A) Temozolomide (TMZ) dose-response curves of control (CTRL, DMSO-treated) and TMZ-resistant (R) U251, U87, U138, and LN18 glioblastoma cell lines following 28 days of treatment with escalating TMZ concentrations. Cell viability was measured after exposure to increasing TMZ doses and IC_{50} values were calculated.
(B) Gene set enrichment analysis (GSEA) comparing transcriptomic profiles of TMZ-resistant and CTRL U87, U251, U138 and LN18 cell lines. Enriched Reactome and Gene Ontology Biological Process (GO-BP) pathways identified in resistant cells are shown.
(C) Representative Annexin V/propidium iodide (PI) flow cytometry plots and quantification of viable (Annexin V^- PI^-), early apoptotic (Annexin V^+ PI^-), late apoptotic/necrotic (Annexin V^+ PI^+), and necrotic (Annexin V^- PI^+) populations following ZIKV infection of CTRL and R cells.
(D) Production of infectious viral particles measured by plaque assay (PFU/mL) following ZIKV infection of CTRL and R GBM cell lines.

(E) Intracellular viral RNA levels quantified by RT-qPCR in CTRL and R cells following ZIKV infection.
(F) Representative LIVE/DEAD fluorescence images and quantification of cell death in U87 CTRL and TMZ-resistant tumor spheres following ZIKV infection. Live cells are shown in green and dead cells in red. Scale bar = 1000 µm.
Data are presented as mean ± SD (n = 3). Each individual symbol represents independent biological replicates. Significance is indicated as *P < 0.05, **P < 0.01, ***P < 0.001, **P < 0.0001; ns, not significant.

Figure 2. Adaptive TMZ responders display increased susceptibility to ZIKV infection and oncolysis

(A) Classification of GBM cell lines according to their response to the TMZ treatment. U251 and U87 cells were classified as adaptive responders (ADA), exhibiting increased TMZ IC_{50} values following chronic TMZ exposure, whereas U138 and LN18 cells were classified as non-adaptive responders (N-ADA), showing no significant change in TMZ response.
(B) Cell viability following ZIKV infection of ADA and N-ADA cell lines at increasing MOI.
(C) Relative cell growth following ZIKV infection in ADA and N-ADA cell lines.
(D) Flow cytometry re-quantification of viable (Annexin V^- PI^-), early apoptotic (Annexin V^+ PI^-), late apoptotic/necrotic (Annexin V^+ PI^+), and necrotic (Annexin V^- PI^+) cell populations following ZIKV infection.
(E) Representative LIVE/DEAD fluorescence images ADA U251, U87 and N-ADA U138 and LN18 cells following ZIKV infection and quantification of cell death at 24, 48, and 72 h post-infection. Live cells are shown in green and dead cells in red. Scale bar = 300 µm.
(F) Quantification of infectious viral particles by plaque assay (PFU/mL) and viral RNA levels following ZIKV infection in ADA and N-ADA cell lines.
(G) Representative immunofluorescence images and quantification of ZIKV infection in GBM cells. Nuclei were stained with DAPI (blue), ZIKV-positive cells are shown in green, and GFAP-positive cells in red. Scale bar = 200 µm.
(H) Quantification of ZIKV-induced cell death in ADA and N-ADA tumor spheres at 24, 48 and 72 h post-infection.
(I) Production of infectious viral particles (PFU/mL) and viral RNA levels in ADA and N-ADA tumor spheres following ZIKV infection.

Data are presented as mean ± SD (n = 3). Each individual symbol represents independent biological replicates. Significance is indicated as *P < 0.05, **P < 0.01, ***P < 0.001, **P < 0.0001; ns, not significant.

Figure 3. MGMT expression and DNA repair-associated transcriptional programs distinguish adaptive and non-adaptive TMZ responses

(A) Relative MGMT mRNA expression measured by RT-qPCR in adaptive responder (ADA; U251 and U87) and non-adaptive responder (N-ADA; U138 and LN18) glioblastoma cell lines. Expression levels were normalized to GAPDH.
(B) Distribution of expression values for genes comprising the MGMT co-expression and DNA repair signatures across ADA and N-ADA cell lines.
(C) Heatmaps of genes associated with MGMT co-expression (left) and DNA repair pathways (right) across ADA and N-ADA cell lines. Rows represent genes and columns represent individual cell lines. Gene expression values are displayed as row-scaled expression levels. Hierarchical clustering was performed using normalized transcriptomic data.
Data are presented as mean ± SD (n = 3). Each individual symbol represents independent biological replicates. Significance is indicated as *P < 0.05, **P < 0.01, ***P < 0.001, **P < 0.0001; ns, not significant.

Figure 4. Patient-derived glioblastoma organoids reproduce the MGMT-dependent ZIKV susceptibility phenotype

(A) Relative MGMT mRNA expression measured by RT-qPCR in GBOs generated from Patient 11947 and Patient 11939. Expression levels were normalized to GAPDH.
(B) Quantification of cell viability following ZIKV infection of GBOs. The infected group was normalized to mock-infected controls.
(C) Production of infectious viral particles following ZIKV infection, quantified by plaque assay (PFU/mL).
(D) Representative immunofluorescence images of ZIKV-infected GBOs. Nuclei are stained with DAPI (blue), ZIKV-positive cells are shown in green, and GFAP-positive cells in red. Scale bar = 100 µm.
Data are presented as mean ± SD. Each symbol represents an individual GBO. Statistical significance is indicated as follows: P < 0.05; ns, not significant.

Figure 5. Pharmacological MGMT inhibition sensitizes the N-ADA cell line LN18 to ZIKV oncolysis through DNA damage accumulation.

(A) Cell viability, assessed by MTT assay and normalised to DMSO vehicle control, in LN18 cells treated with iMGMT (50 µM) alone, ZIKV (MOI 0.5) alone, or their combination at 72 h post-infection.
(B) ZIKV viral production, measured by RT-qPCR of viral RNA in culture supernatants (viral particles/µL), in LN18 cells infected with ZIKV (MOI 0.5) alone or in combination with the MGMT inhibitor O⁶-benzylguanine (iMGMT, 50 µM) at 72 h post-infection.
(C) Quantification of mean γH2AX signal per nucleus in LN18 cells treated with iMGMT (50 µM), ZIKV (MOI 0.5), or their combination, assessed by immunofluorescence. Each dot represents an individual nucleus.
(D) Representative immunofluorescence images of LN18 cells treated as in (C), stained for DAPI (blue) and γH2AX (red). The right column shows magnified views of the boxed regions in the left column. Scale bar: 300 µm.

Data are presented as mean ± SD from 2 independent experiments. *p < 0.05, **p < 0.01, ***p < 0.001; ns, not significant.

Abbreviations: iMGMT, O⁶-benzylguanine (MGMT inhibitor); MOI, multiplicity of infection; γH2AX, phosphorylated histone H2AX.

8. Figures

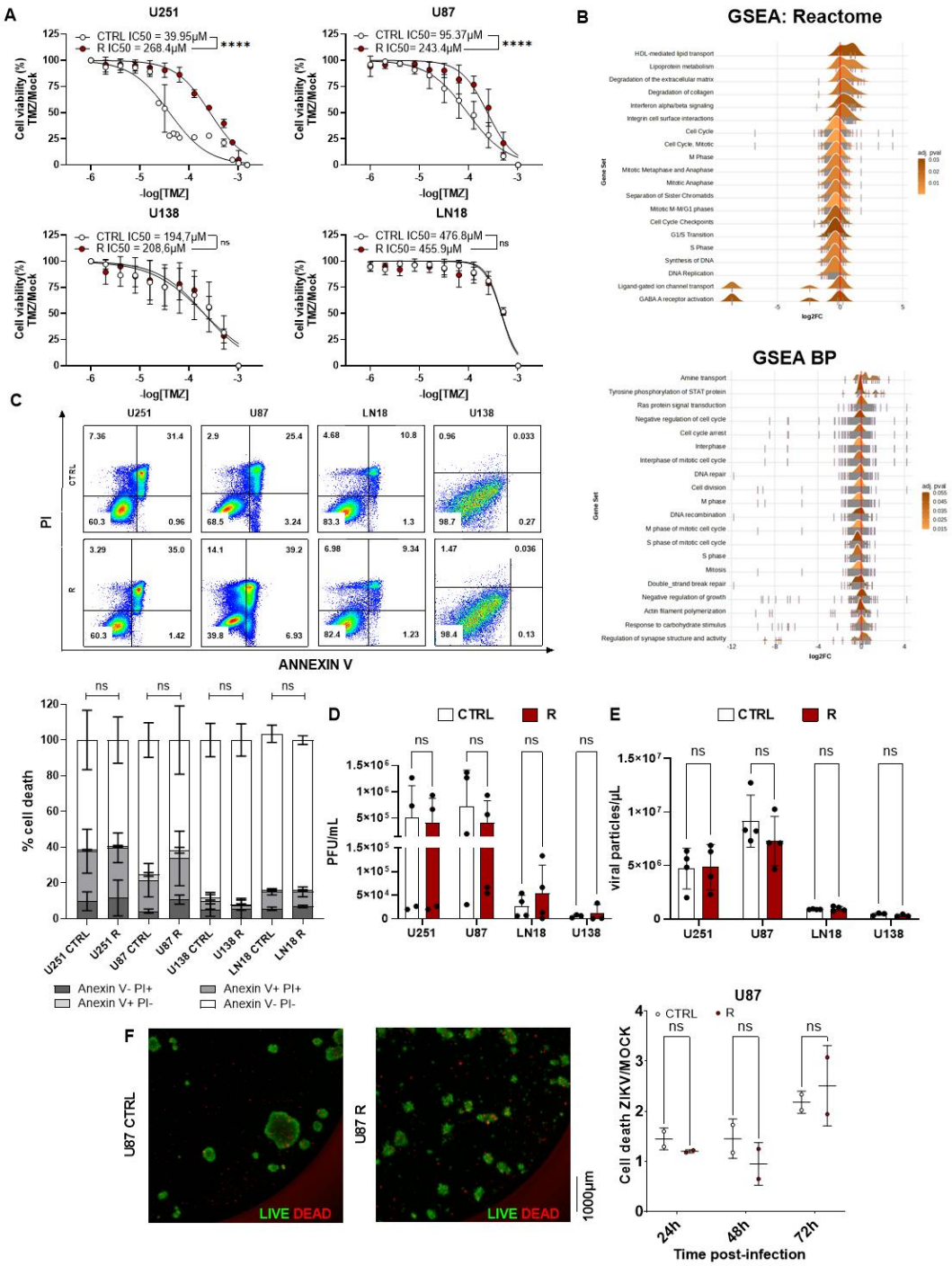

A
U251
CTRL IC50 = 39.95µM
R IC50 = 268.4µM
****
U87
CTRL IC50= 95.37µM
R IC50= 243.4µM
****
U138
CTRL IC50 = 194.7µM
R IC50 = 208.6µM
ns
LN18
CTRL IC50= 476.8µM
R IC50= 455.9µM
ns
Cell viability (%) TMZ/Mock
-log[TMZ]
B
GSEA: Reactome
HDL-mediated lipid transport
Lipoprotein metabolism
Degradation of the extracellular matrix
Degradation of collagen
Interferon alpha/beta signaling
Integrin cell surface interactions
Cell Cycle
Cell Cycle, Mitotic
M Phase
Mitotic Metaphase and Anaphase
Mitotic Anaphase
Separation of Sister Chromatids
Mitotic M-M/G1 phases
Cell Cycle Checkpoints
G1/S Transition
S Phase
Synthesis of DNA
DNA Replication
Ligand-gated ion channel transport
GABA A receptor activation
Gene Set
adj. pval
log2FC
GSEA BP
Amine transport
Tyrosine phosphorylation of STAT protein
Ras protein signal transduction
Negative regulation of cell cycle
Cell cycle arrest
Interphase
Interphase of mitotic cell cycle
DNA repair
Cell division
M phase
DNA recombination
M phase of mitotic cell cycle
S phase of mitotic cell cycle
S phase
Mitosis
Double-strand break repair
Negative regulation of growth
Actin filament polymerization
Response to carbohydrate stimulus
Regulation of synapse structure and activity
C
U251
U87
LN18
U138
CTRL
R
PI
ANNEXIN V
7.36
31.4
60.3
0.96
2.9
25.4
68.5
3.24
4.68
10.8
83.3
1.3
0.96
0.033
98.7
0.27
3.29
35.0
60.3
1.42
14.1
39.2
39.8
6.93
6.98
9.34
82.4
1.23
1.47
0.036
98.4
0.13
% cell death
ns
U251 CTRL
U251 R
U87 CTRL
U87 R
U138 CTRL
U138 R
LN18 CTRL
LN18 R
Anexin V- PI+
Anexin V+ PI-
Anexin V+ PI+
Anexin V- PI-
D
CTRL
R
PFU/mL
U251
U87
LN18
U138
E
CTRL
R
viral particles/µL
U251
U87
LN18
U138
F
U87 CTRL
U87 R
LIVE DEAD
1000µm
U87
CTRL
R
Cell death ZIKV/MOCK
24h
48h
72h
Time post-infection

Figure 1. Acquisition of temozolomide resistance does not alter susceptibility of GBM cells to ZIKV infection

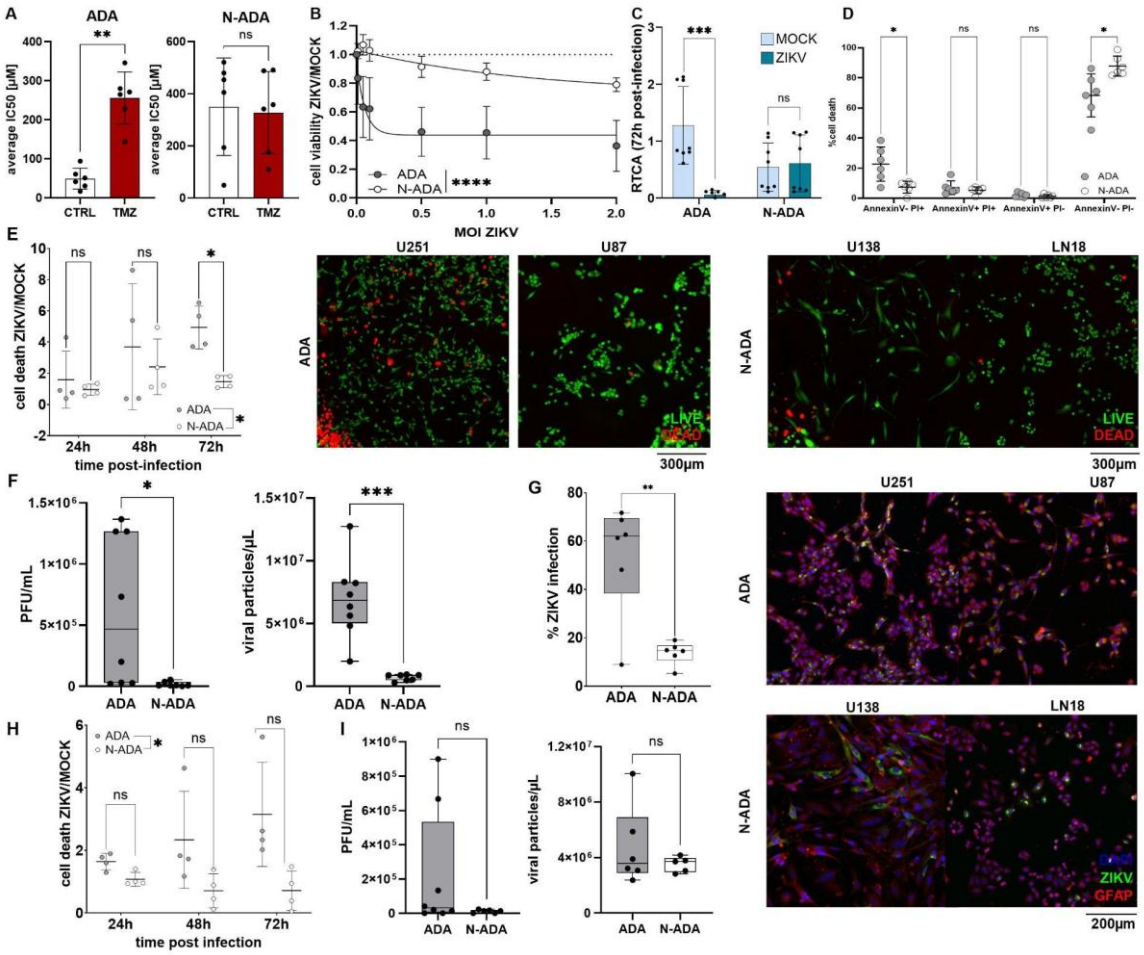


Figure 2. Adaptive TMZ responders display increased susceptibility to ZIKV infection and oncolysis

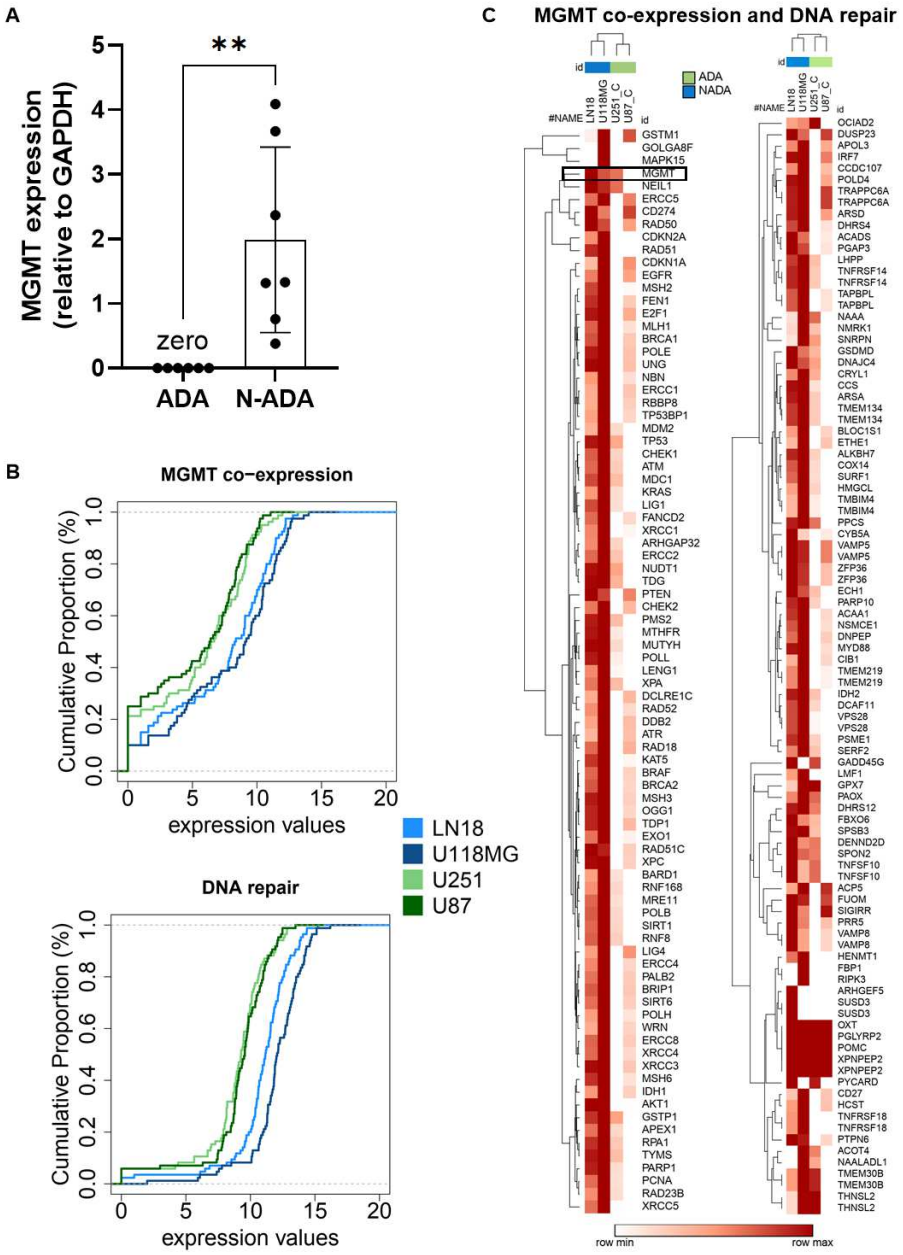


Figure 3. MGMT expression and DNA repair-associated transcriptional programs distinguish adaptive and non-adaptive TMZ responses

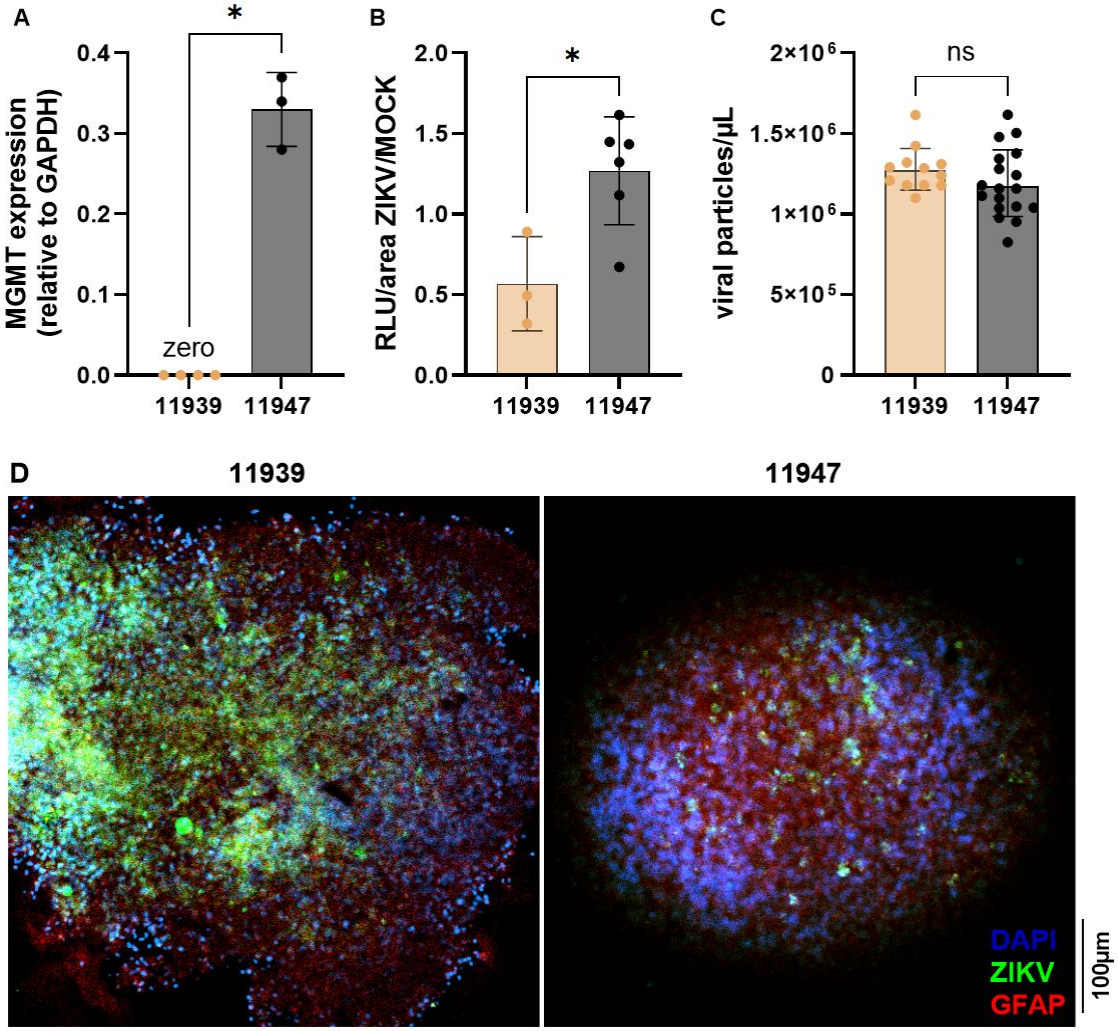


Figure 4. Patient-derived glioblastoma organoids reproduce the MGMT-dependent ZIKV susceptibility phenotype

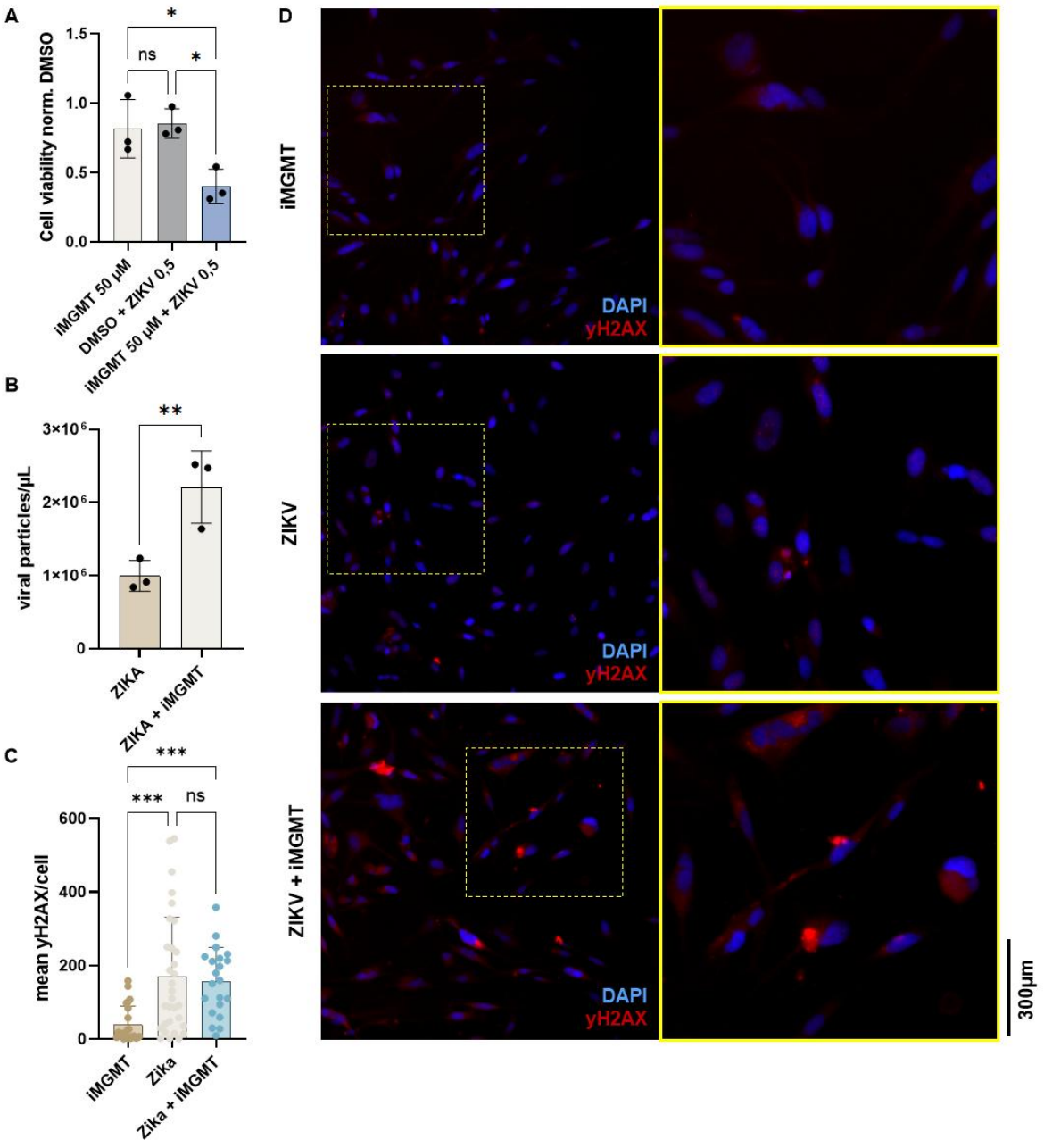


Figure 5. Pharmacological MGMT inhibition sensitizes the N-ADA cell line LN18 to ZIKV oncolysis through DNA damage accumulation.

Supplementary Files

This is a list of supplementary files associated with this preprint. Click to download.

- GranhaZIKVMGMTGBMSupplementarytablesJNO.docx
- GranhaZIKVMGMTGBMSupplementaryMethodsJNO.docx
- GranhaZIKVMGMTGBMSupplementaryfiguresJNO.docx